Measurement 174 (2021) 109017

Contents lists available at ScienceDirect

Measurement

journal homepage: www.elsevier.com/locate/measurement

High-sensitivity gas leak detection sensor based on a compact microphone array

Jian Li [a,b], Yulin Li [a,b], Xinjing Huang [a,b,*], Jiahao Ren [a,b], Hao Feng [a,b], Yu Zhang [a,b], Xiaoxia Yang [c]

[a] State Key Laboratory of Precision Measuring Technology and Instruments, Tianjin University, Tianjin 300072, China
[b] Binhai International Advanced Structural Integrity Research Centre, Tianjin 300072, China
[c] Tianjin Key Laboratory of Information Sensing & Intelligent Control, Tianjin University of Technology and Education, Tianjin 300222, China

ARTICLE INFO

Keywords:
Acoustic sensor
Leak detection
Tiny gas leak

ABSTRACT

Early detection of tiny leaks in gas-pressurized vessels and pipelines can prevent disasters. Algorithm and sensor developments can enable acoustic methods to achieve high-sensitivity online leak detection by monitoring the sound generated by a leak and propagating in air. In this study, a compact MEMS microphone array-based sensor is proposed to detect very small gas leaks. Numerical calculation and experiment results show that the sensor gain (compared to a single microphone) is equal to the array element number when the azimuth of the leak source relative to the sensor is close to 0°. The proposed sensor can detect leaks as small as 0.67 mL/s emitted from a 0.1 mm hole at a distance of 20 cm. The bubble method can be used to enable the sensor to detect even smaller leaks, as low as 0.1 mL/s, at a distance of 10 cm using the burst sound of an invisible bubble.

1. Introduction

Gas-pressurized vessels and pipelines are ubiquitous in the field of oil and gas storage and transportation, as well as industrial production. Leakage poses a high risk of grave accidents, such as poisoning, fire or explosion. Therefore, the rapid detection of the existence and location of leaks, as well as the distribution and dynamics of the leaked gas, is extremely important to prevent leak-induced disasters. Countries all over the world have placed considerable importance on the development of gas leak detection technology and instruments.

Infrared thermal imaging is typically employed to monitor the diffusion of leaked gas in air, wherein the radiation intensity or radiation spectrum for a specific infrared band in the target area of the gas leak is used to identify a gas leak [12]. There are two types of thermal imaging methods: active imaging based on laser source radiation absorption and passive imaging based on background radiation absorption. Thermal imaging methods offer the advantages of high efficiency, a large detection area and dynamic visualization. Chromatographic methods can also be used to detect leaked gas by measuring the concentration of sensitive substances in an air sample collected in the monitored area [3].

Leaks in pipelines and vessels used for pause production can be detected using helium mass spectrometry with a suction gun or the bubble method by checking the airtightness of the vessel. The helium mass spectrometer method involves covering the exterior of the vessel under inspection with plastic film to create a local seal, followed by charging the vessel with pressurized helium. A suction gun is inserted into the plastic film for sampling. A helium mass spectrometer reading above the background indicates a gas leak in the detection area [4,5]. The bubble method involves filling the vessel under inspection with pressurized air. Foaming liquid is applied to the detection area. Leakage is indicated by the formation of a large number of visible bubbles, the size and frequency of which indicate the degree of leakage [6].

Leaks in pressurized vessels generate elastic waves that propagate in the vessel wall and sound waves that propagate in air. Leaks in in-service vessels can be monitored and located online by capturing these elastic and sound waves, corresponding to the acoustic emission method and acoustic wave method, respectively. The acoustic emission method is a contact technique, whereby a sensor pasted on a vessel wall receives elastic waves generated by the leak. The elastic waves are converted into electrical signals that are collected by a computer, and signal processing is used to detect leaks [7,8]. The acoustic wave method is a noncontact technique, whereby a leak is detected by collecting and analyzing the wideband of the leak sound that has diffused in air. The leak sound is independent of the type of leaked material and can propagate over a

* Corresponding author at: State Key Laboratory of Precision Measuring Technology and Instruments, Tianjin University, Tianjin 300072, China.
E-mail address: huangxinjing@tju.edu.cn (X. Huang).

https://doi.org/10.1016/j.measurement.2021.109017
Received 31 August 2020; Received in revised form 6 January 2021; Accepted 9 January 2021
Available online 17 January 2021

long distance. As most gas vessels are pressurized, a leak inherently generates sound waves. The merits presented above have resulted in the widespread use of acoustic leak detection methods [9,10].

Considerable effort has been expended in developing algorithms and sensors to enhance the sensitivity and localization accuracy of acoustic leak detection methods, [11]. Mengjie X et al. [12] used an ultrasonic sensor array to estimate the leak position based on differences in the acoustic arrival time. Cruz R P [13] used a machine learning algorithm to reduce the false alarm rate in the presence of external interference and improved positioning accuracy. Yuxing Li [14,15] used a time-frequency analysis to distinguish acoustic signals generated by leaks from background noise, modified the calculation formula of the leak position to improve positioning accuracy, and was able to detect and locate a leak from a Φ0.1-mm hole. Hao Jin [16] improved the calculation formula for the sound velocity and leak localization, as well as a wavelet double-threshold denoising optimization algorithm, to effectively improve the localization accuracy and correctness rate of pipeline leak detection. Wang S et al. [17] used the Lighthill acoustic analogy to establish a basic measurement principle and applied the finite element method to calculate the fitting parameters of leak rate equations: the results were used to detect a 10 L/min (166.6 mL/s) leak.

It is also important to improve the hardware performance of an acoustic leak detection system to enhance detection sensitivity and positioning accuracy. Li L et al. [18] designed a virtual linear ultrasonic transducer array of only two transducers to acquire leak signals; a virtual beamforming algorithm based on the mutual power spectrum was used to accurately and reliably locate gas leaks. Qi Lei et al. [19] developed a noncontact ultrasonic system to detect gas leakage from a Φ0.3-mm hole with a 500-mm maximum detection distance. Guo Xin et al. [20] designed an ultrasonic leak detection device that can detect leaks at rates above 1.6 Pa·m^3/s (15.8 mL/s @ 1 atm). Leaks with rates greater than 1.0 Pa·m^3/s (9.9 mL/s @ 1 atm) can be detected and located under contact conditions.

A low-cost, high-sensitivity gas leak detection sensor based on a small, compact MEMS microphone array is proposed in this study. First, the working principle and gain directivity of the sensor are analyzed. Sound receiving experiments are then performed to test the frequency response consistency and gain directivity of the sensor. Finally, comprehensive experiments are conducted to demonstrate the high sensitivity of the sensor for detecting small gas leaks at rates below 1 mL/s.

2. Design of microphone array-based sensor

A schematic, a photograph, and a PCB schematic of the sensor are shown in Fig. 1. The output signals of each MEMS microphone pass through a DC blocking circuit and are then superimposed by the adder circuit as the final sensor output. The output of each microphone is first connected in series with a DC blocking capacitor and is then connected in series with a resistor. This resistor is connected to the noninverting input of an operational amplifier. A feedback resistor R_f is connected between the output of the operational amplifier and the inverting input terminal, and a resistor R_g is connected between the inverting input terminal and the ground. The microphone outputs are superimposed by a noninverting amplifier circuit, which is shown as a schematic in Fig. 1 (c). The sensor output u_0 is given by Eq. (1), where the output signal of each microphone is denoted by u_i.

$$u_0 = \sum_{i=1}^{N}\left(1+\frac{R_f}{R_g}\right)\left(u_i \times \frac{R_1//\cdots//R_{i-1}//R_{i+1}//\cdots//R_N}{R_i + R_1//\cdots//R_{i-1}//R_{i+1}//\cdots//R_N}\right) \quad (1)$$

The sensor employs a small MEMS silicon microphone chip AM4311T42A0 with a sensitivity of 7.58 mV/Pa. The sensor sensitivity is greater than 85 mV/Pa for directional angles less than 45°. For other microphone chips, such as the SPU0410LR5H-QB and SPV0842LR5H-1, the acoustic hole is located at the bottom of the chip in the same plane as

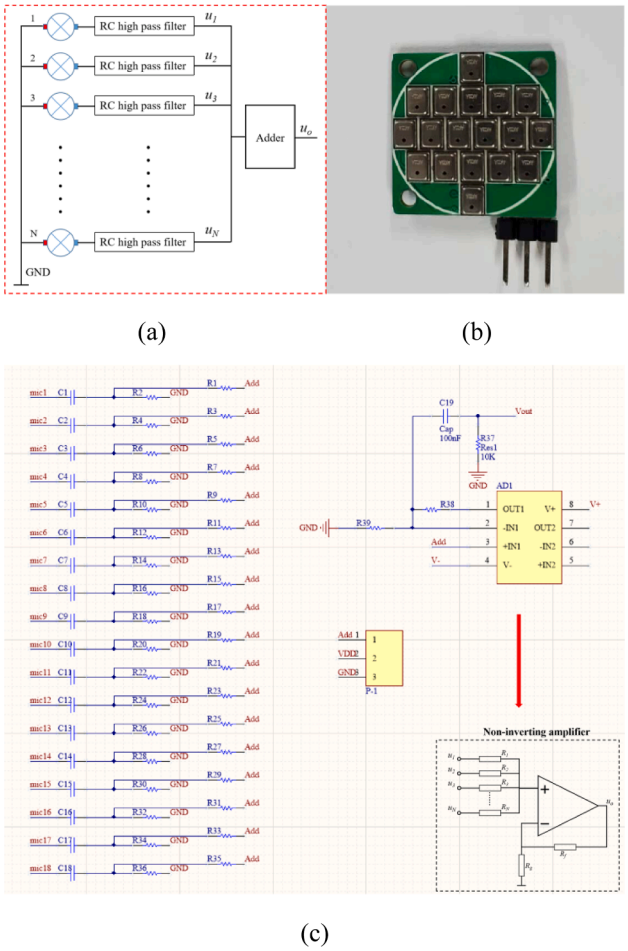

Fig. 1. Working principle of mic array sensor: (a) sensor schematic; (b) photograph; (c) schematic of noninverting amplification circuit.

the pad; thus, an open hole in the PCB board is require to collect sound, which affects the acoustics, while and taking the space of many sensors, and is therefore not a suitable design for small sensors. The acoustic hole of the AM4311T42A0 microphone chip used in this study is located at the front of the chip, obviating an opening in the PCB board. A digital microphone chip outputs a digital signal that must be collected and processed by FPGA to sum all the signals of the mic array. In addition, the narrow bandwidth of a digital microphone chip cannot be used to acquire high-frequency leakage sound signals.

The leak sound is broadband: the frequency components of the leak sound have different wavelengths, and there is a phase difference between the output signals of each microphone element, which affect the total output amplitude. Therefore, the outputs of microphone arrays with different layouts must be calculated numerically. As the probe is considerably smaller than the distance between the probe and the leak sound source, the leak sound can be considered to propagate over the same distance to each microphone, and the output amplitudes of the microphones can be considered to be equal. The phase of the output signal of the microphone at the center of the array is used as a reference. The leak generates a broadband acoustic signal. The output signal of the i-th microphone by s_i is expressed as

$$s_i = \sum_{j=1}^{m} A_j sin(\omega_j t + \phi_{ij}), \quad (2)$$

where j is the frequency number, $f_j = \omega_j/2\pi$ is the leak sound frequency, and A_j is the corresponding amplitude. φ_{ij} is the relative initial phase, which is different for acoustic signals of different frequencies for microphones. φ_{ij} is calculated as follows:

$$\varphi_{ij} = 2\pi \cdot \frac{(l_0 - l_i)}{c/f_j}, \tag{3}$$

where c is the speed of sound in air, l_0 is the length of the sound path from the leak point to the center of the array, and l_i is the length of the sound path from the leak point to the i-th microphone. The superimposed signal s_j for leak sound frequency f_j is

$$s_j = \sum_{i=1}^{n} A_j sin(\omega_j t + \varphi_{ij}). \tag{4}$$

It should be noted that various amplitudes/phases were not directly added, instead, the waveforms containing amplitude and phase information of each microphone were added, as shown by Eqs (2)–(4). The output of each microphone was not amplified, but the circuit adder plays an amplification role. By dividing the output of the mic array by that of single microphone, the real gain of the proposed sensor can be obtained. Passive filtering and direct addition of the microphone output signal were adopted to effectively avoid the noise caused by the introduction of active circuits while improving the sensitivity of the mic array sensor. The white noise of the output signal of a single microphone is summed and then canceled by each other, which can reduce the noise floor and improve the signal-to-noise ratio of the sensor output signal. However, adding would also result in the cancellation since some of these signals are out of phase. Therefore, gain comparison of different arrays considering the phase information of each microphone is carried out via numerical calculations and experiments.

2.1. Gain comparison for different arrays

Fig. 2 shows the results of a numerical calculation used to perform a gain comparison of different arrays, considering the phase information of each microphone. The leak sound source is assumed to lie along a line 1 m in front of the array, and the sound source moves from the front of the array to the right. The moving distance is x. Considering that the sound source with different frequencies is moving, the output of the microphone array is recorded at different moving distances and analyzed.

When x gradually increases from 0 m to 1 m, the azimuth angle β of the leak sound source relative to the array gradually increases from 0° to 45°. The leak sound source is assumed as a point source. The output gains of three arrays were calculated, and the size and layout of each array is shown in Fig. 2. Considering that the low-frequency noise in the field is large, the frequency range of the test is set to a middle-high frequency range of 10–30 kHz, which covers both the frequency response range of the microphone and the spectrum of the leak induced sound. In the calculation, it is assumed that the frequency response curve of each microphone is the same, and the gain of a single microphone is regarded as 1. The calculated array gain is shown in Fig. 3.

For all the three mic array sensors, it can be seen from Fig. 3 that all

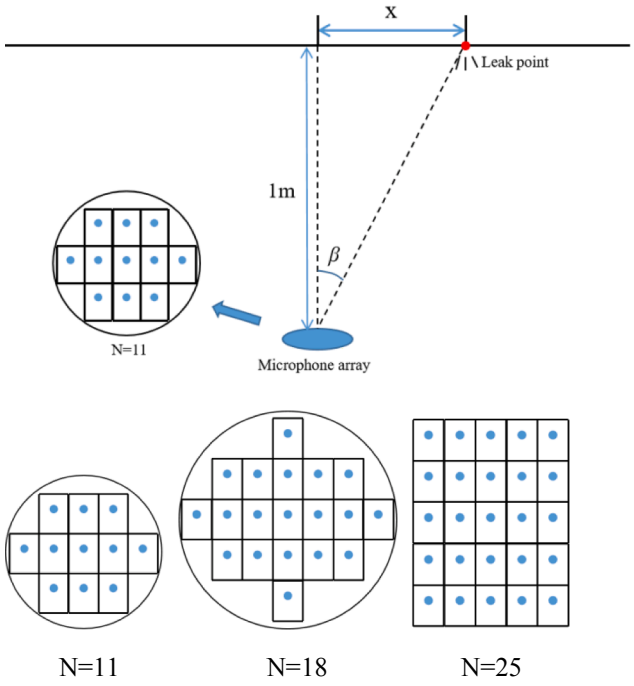

Fig. 2. Numerical calculation configurations.

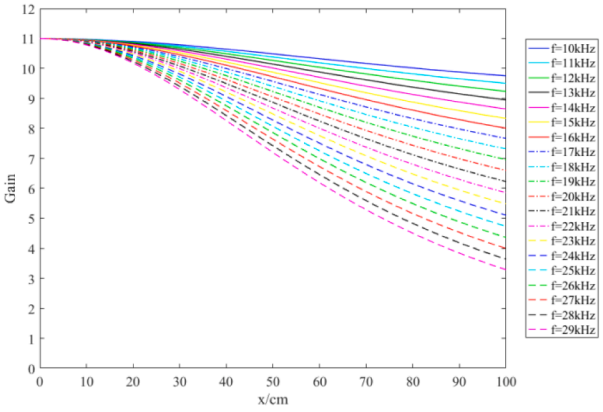

(a) N=11

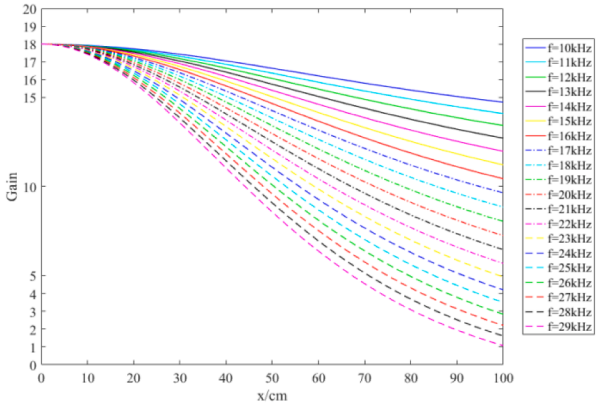

(b) N=18

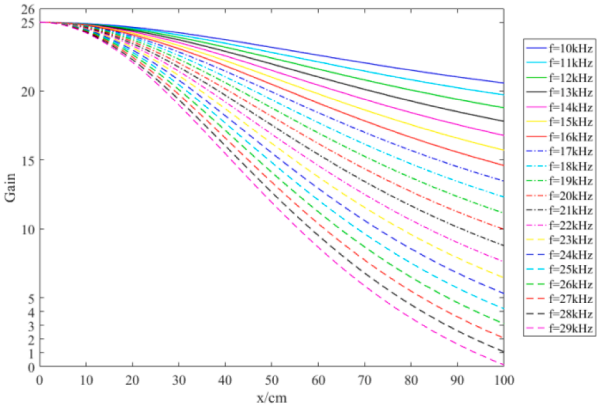

(c) N=25

Fig. 3. Gains of different arrays.

the three have a maximum gain of N when the leak sound source is in front of the array; N is the number of the microphones. And the maximum gain can be maintained within the azimuth angle of $\pm 5^\circ$ ($x = \pm 8.8$ cm). As the leak sound source gradually deviates to 1 m and the azimuth angle tends to be 45° ($x = 100$ cm), the gain becomes smaller, and the minimum gain decreases as the number of array elements increases. For each array, the lower the leak sound frequency is, the slower the gain decreases as the leak source deviates to the side. When the frequency is 20 kHz (median of the tested frequencies), the sensor has a gain of $N/\sqrt{2}$ for an azimuth β of less than about 30°; Specifically, if $x = 73$ cm and $N = 11$, $\beta = 36^\circ$; if $x = 51$ cm and $N = 18$, $\beta = 27^\circ$; if $x = 53$ cm and $N = 25$, $\beta = 28^\circ$.

3. Sensor performance test

The experimental apparatus is shown in Fig. 4. The sensor is fixed on a slider placed on a table. A broadband loudspeaker is used to play sounds of different frequencies. The loudspeaker is placed on a height-adjustable lifting platform to maintain the sound source and the sensor at the same height. The slider can be moved along the x direction to adjust the azimuth angle of the sound source relative to the sensor to verify the numerically calculated directivity. The relative positions of the sensor and the sound source are shown in Fig. 4. A separate microphone is pasted on the open space next to the sensor. The array sensor and the single microphone are moved with the slider, and the ratio of the output of the sensor to that of the microphone is the sensor gain. The consistency of the output amplitude of the sensor was also tested, and the result is shown in Fig. 5. The gain directivity test results are shown in Fig. 6.

3.1. Consistency

Sixteen sensors were fabricated, and their frequency response characteristics were tested. Each sensor was placed in front of the loudspeaker at the same height as the loudspeaker. The frequency sweep ranged from 10 kHz to 25 kHz, with a 1 kHz step size. The mean and standard deviation of the output signals of the 16 sensors were calculated for each test frequency, and the frequency response curve and standard deviation of the sensors are plotted in Fig. 5. The statistical results show that the standard deviation is 9.8%-15.4% of the amplitude with an average relative fluctuation of 12.2%, that is, the sensors exhibit good consistency. The frequency response curve is similar in shape to the frequency response curve of the MEMS microphone provided by the datasheet, and the microphone used by the sensor is highly sensitive over the 14–17 kHz frequency range. As the gas leak sound is broadband, the sound signal of this frequency band can be used to identify a leak.

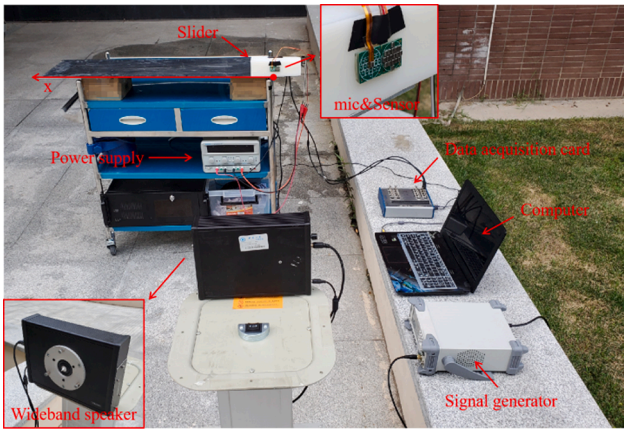

Fig. 4. Sensor performance test apparatus.

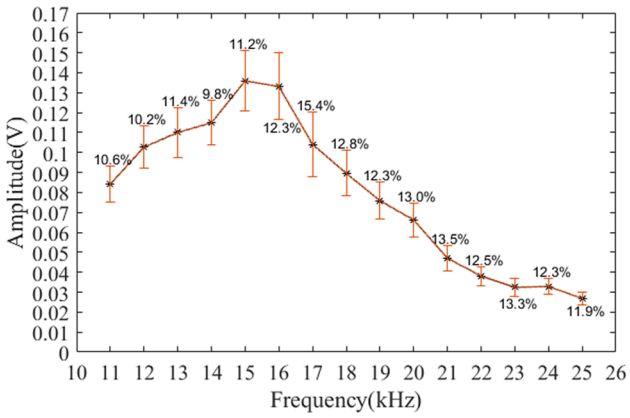

Fig. 5. Frequency response test results.

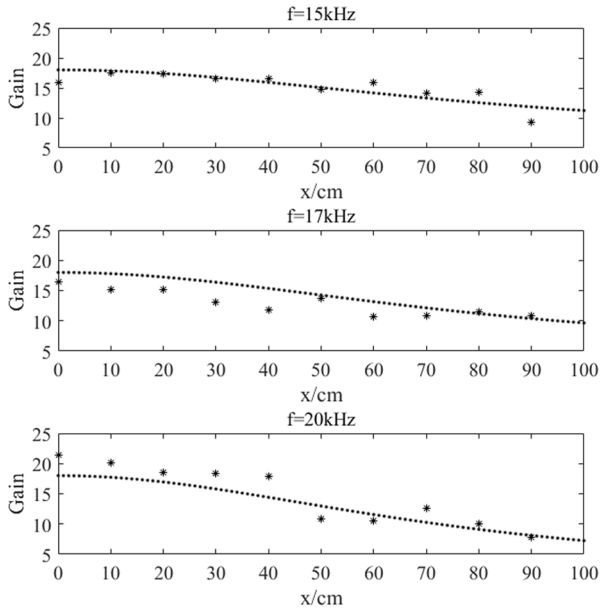

Fig. 6. Directivity test results.

3.2. Directivity

The position of the mic array in front of the loudspeaker is recorded as $x = 0$ cm. As the sensor moves laterally, the output signal of the sensor is collected as well as that of the separate single microphone. Signals were recorded when the sensor was moved to the locations with an adjacent interval of 10 cm. High frequency acoustic signals of 15 kHz, 17 kHz and 20 kHz were collected. The directivity gain of the array at different frequencies was obtained by calculating the ratio of the output amplitude of the mic array to that of the single microphone, and is compared with the numerical calculation results of directivity gain. The results are shown in Fig. 6. In the process of moving the slider, the attitude of the slider slightly changed, and the array output amplitude had some fluctuation, so the measured gain was not so smooth as the calculated one. The directivity test at different frequencies was carried out for many times and the gains were averaged; the results are shown by those points in Fig. 6. The curves in Fig. 6 are the directivity curves obtained by numerical calculation. It can be seen that the experimental results conform to the curves numerically calculated.

4. Leak detection applications

4.1. Test method

The gas leakage rate is an important index of the performance of a sealed device and an important parameter for testing the sensitivity of a leak detection device [21]. Leak sound signals with different leak rates were collected using the proposed sensor. The leak detection test equipment is shown in Fig. 7. Air was prefilled into a stainless steel tank to an internal pressure above the room atmospheric pressure. The compressed air from the pressure tank was sent through a hose to a stainless steel leak device. The volume of the gas tank was 1 L. A small leak hole was machined on the end face of the leak device, and a total of four types of leak devices with Φ0.1 mm, Φ0.2 mm, Φ0.3 mm and Φ0.5 mm holes were manufactured. The leak test was performed by opening the leak valve to allow gas to naturally escape, such that the tank pressure gradually decreased to zero. The gas leak rate was calculated from the pressure change in the gas tank over time, as given below [22].

The ideal gas state equation is:

$$pV = nRT = \frac{m}{M}RT \tag{5}$$

where, p is the air pressure, V is the volume of the gas, n is the amount of substance, R is the gas constant, T is the absolute temperature, m is the mass of the gas, and M is the average relative molecular mass of air.

Assuming that a gas tank with volume V_0 and ambient temperature T_0 is leaking and the external pressures at temperatures t_1 and t_2 are p_1 and p_2, the mass of the leaked gas is

$$\Delta m = \frac{MV_0}{RT_0}(p_2 - p_1) \tag{6}$$

After the gas leaks into the atmosphere, the leaked gas has a volume of

$$\Delta V = \frac{RT_0}{Mp_0}\Delta m = \frac{p_2 - p_1}{p_0}V_0 \tag{7}$$

Wherein, p_0 is the room atmospheric pressure. The average leak rate over this period is

$$Q = \frac{V_0}{p_0}\frac{p_2 - p_1}{t_2 - t_1} \tag{8}$$

Fig. 8 is a flowchart showing the experimental procedure and algorithm used for sensor performance testing and evaluation. After setting up the apparatus for the leak detection experiments, the leakage aperture is chosen and assembled, and the gas tank is pressurized to more than 100 kPa. The leak valve is opened, and the gas leaks freely. The acoustic leak signal and the pressure change are simultaneously recorded. Then, the leakage aperture and detection distance are changed, and the experiment is repeated. The recorded data is processed to obtain the variation in the pressure with time, and the resulting curve is fitted. The leak rate-time relationship is obtained from the pressure-time relationship using Eq. (8). The leak signal in the time domain signal is fast Fourier transformed to obtain the signal in the frequency domain, from which the 13 kHz to 15 kHz band information is extracted and averaged to obtain the average amplitude-time relationship of the leakage sound. Finally, the leak rate-time and average amplitude-time graphs are plotted.

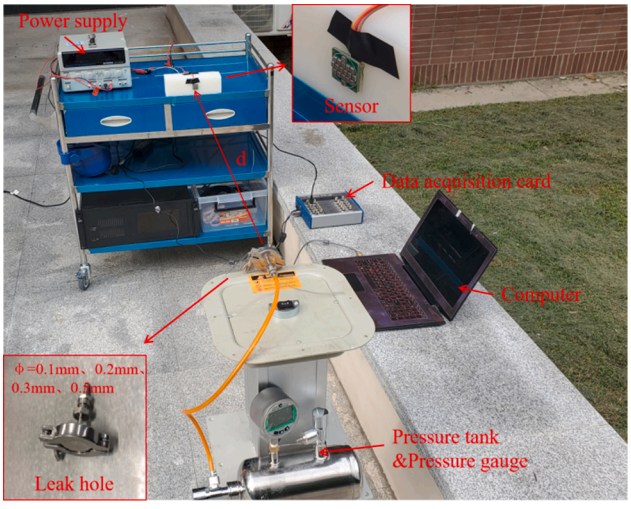

Fig. 7. Leak detection test apparatus.

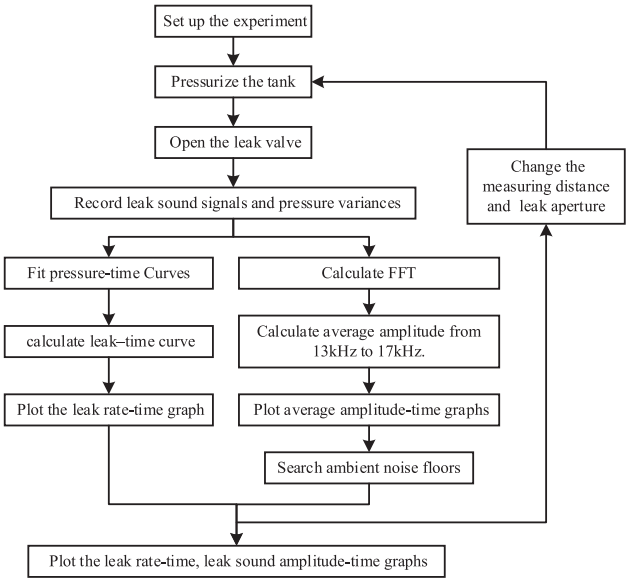

Fig. 8. Flowchart for experimental procedure and algorithm for sensor leak detection performance test.

4.2. Tiny leak detection test

The change in the gas tank pressure was recorded during

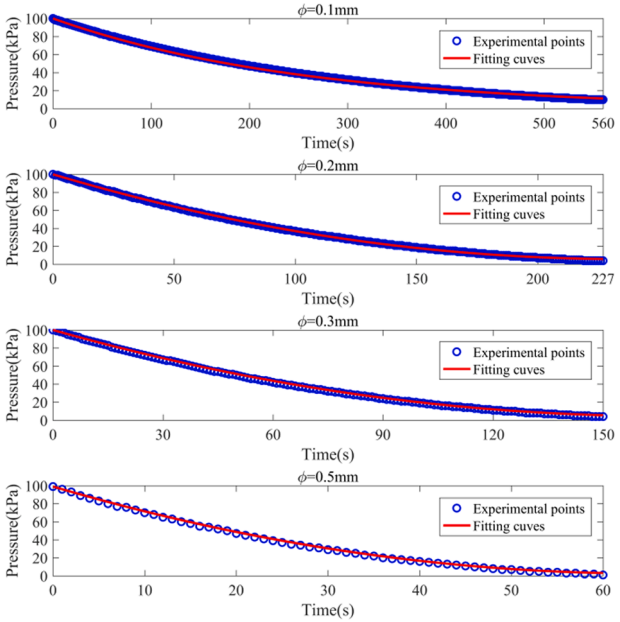

Fig. 9. Pressure drop in pressurized gas tank for different leak holes.

experiments performed using the four leak holes and is shown in Fig. 9. The raw pressure data were fitted and the leak rate was calculated using Eq. (4). The calculated leak rate corresponds to the blue curves shown in Fig. 10. Six scenarios were tested: $d = 20$ cm, leak hole diameter $\Phi = 0.1$ mm; $d = 20$ cm, 50 cm and 100 cm, $\Phi = 0.2$ mm; $d = 100$ cm, $\Phi = 0.3$ mm; and $d = 100$ cm, $\Phi = 0.5$ mm. The tank pressure gradually decreased as the gas escaped from the tank, and the resulting leak sound was recorded. The frequency response test result presented in Fig. 5 shows that the sensor has a high sensitivity in the 13–17 kHz frequency range. The average amplitude V_a in the frequency domain of the leak sound over this frequency range was calculated and used as a characteristic parameter to identify leaks. The V_a-time relationship curve corresponds to the red curves shown in Fig. 10. The average amplitude of ambient noise in the same frequency range, V_n, was also calculated and is plotted in Fig. 10.

It can be seen from Fig. 10 that the intensity of the leak sound decreases as the leak rate decreases. When the leak rate is reduced to a certain value, the intensity of the sound no longer changes. In other words, the amplitude of the leak sound received by the mic array sensor is lower than the ambient noise amplitude and the sensor cannot detect the leak. The leak rate at this point is the lower limit of leak detection. The lower limits of leak rate detection for different test conditions such as leak holes and distances are summarized in Table 1. It is worth noting that at a fixed distance, the sensor can detect smaller leak from a smaller leak hole, namely, a smaller leak hole generates a larger leak sound. It can be found that the sensor at a distance of 50 cm from the leak location can detect the leak sound caused by a leak from a Φ0.2 mm hole when the leak rate is larger than 1.7 mL/s; at a distance of 20 cm from the leak location the sensor can detect the leak sound caused by a leak from a Φ0.2 mm hole when the leak rate is larger than 0.8 mL/s; at a distance of 20 cm from the leak location the sensor can detect the leak sound caused by a leak from a Φ0.1 mm when the leak rate is larger than 0.67 mL/s. In addition, some examples of small leak sound and ambient noise spectra are displayed in Fig. 11. It can be seen that the leak sound signal is broadband, and its amplitude is higher than the background noise in the entire frequency band.

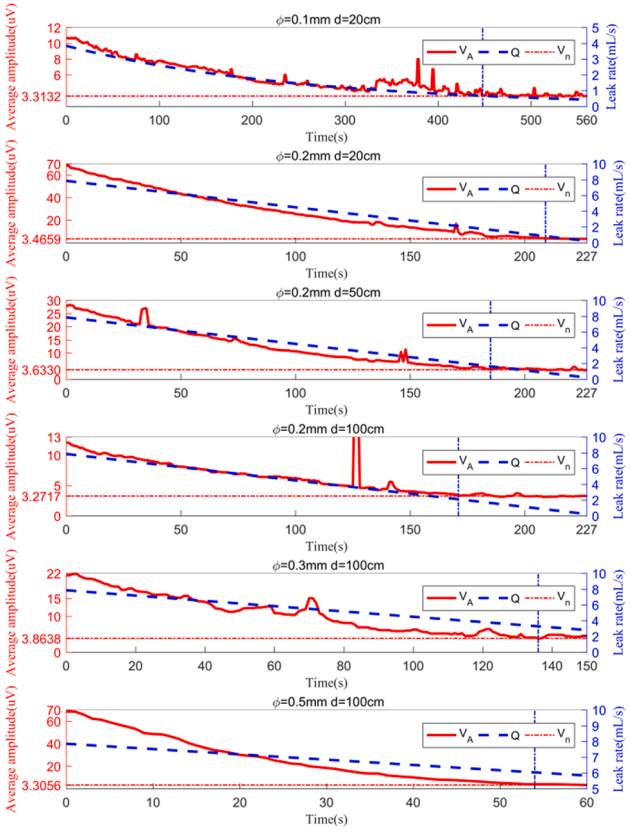

Fig. 10. Variation in leak sound amplitude and leak rate under different test conditions.

Table 1
Leak detection threshold under different conditions.

Φ/mm	Distance/cm	Time slice/s	Leak rate/mL/s
0.5	100	54–55	5.27
0.3	100	136–137	3.28
0.2	100	171–172	2.07
0.2	50	185–186	1.64
0.2	20	209–210	0.83
0.1	20	448–449	0.67

Pulse interferences can be observed in Fig. 10. These pulses originate from man-made environmental noise that appeared during the experiment. These pulses are transitory, whereas a leak sound is relatively long term, especially from a pressurized field vessel whose pressure does not decrease for a small leak. Therefore, these pulses do not affect the small-leak detection results or the lower limit of leakage detection. The amplitude directivity of the proposed array sensor has a maximum gain when the leak point azimuth is 90° and a very small gain, even reduction gain, when the leak point azimuth is near 0 or 180°. The sensor has a high amplitude when the sound source is in front of the sensor, i.e. the azimuth is between 90° ± 30°, whereas a sound signal at the side of the sensor is suppressed. Therefore, we can use the directivity of the proposed sensor to suppress broadband background noise.

4.3. Leak bubble burst detection

A gas leak with an excessively low rate cannot generate a sufficiently large sound to be detected by the proposed sensor. Therefore, the bubble method is used to physically amplify the leak sound. The surface of the leak hole is evenly smeared with an ultrasonic amplification fluid with a large surface tension, and the leak hole is then completely immersed in the fluid. The Φ 0.1-mm demo leak hole produces a leak rate of 0.1 mL/s, which is considerably smaller than the detection limit, as shown in Table 1. A syringe is used to generate a 0.1 mL/s gas leak. As the plunger of the syringe is slowly pushed forward, air bubbles form on the surface of the leak hole, and the resulting bubble burst amplifies the leak sound.

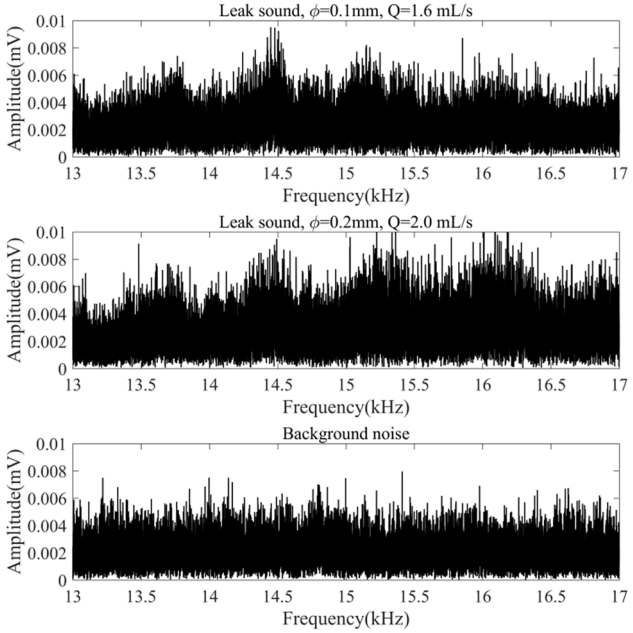

Fig. 11. Examples of leak sound and background noise spectra.

The sensor is placed directly above the leak hole, and the distance between the sensor and the leak hole is adjusted to 1 cm, 3 cm, 5 cm, 7 cm, 9 cm, and 10 cm. Although the bubble is too small to be visible, the sound of the burst can be detected by the proposed sensor. The output signals were collected and the response of the microphone array was analyzed.

Fig. 12 shows the original waveforms of bubble burst sound collected by the sensor at different distances. The signals in red box in the figure is the sound signal of bubble burst. It can be clearly seen that if the detection distance is shorter than 10 cm, the sensor can sensitively capture the leak sound signal generated by the 0.1 mL/s gas leak. At different distances, the amplitude of the bubble bursting sound is different and random, which is related to the size of the bubble when bursting. The bubble burst sound collected when the distance is 10 cm is taken as an example. The time-domain waveform and the frequency spectrum of the leak sound, and the frequency spectrum of the environmental noise are shown in Fig. 13. It can be seen that the bubble burst sound is an attenuated sine wave of which the frequency is around 15 kHz, while the background noise spectrum does not have any characteristic peaks.

4.4. Quantitative comparison with other work

There are many applications that use acoustic methods to detect gas leaks. The applications all achieve improved leak detection performance via hardware and/or algorithm improvements. Qualitative comparisons between other results of acoustic leak detection methods and this work are listed in Table 2. It can be found that most of these applications detect leaks with large apertures and large differential pressures, resulting in large leak rates. For example, Qi Lei et al. [19] achieved the detection of gas leakage with an aperture of 0.3 mm; Mengjie X et al. [12] achieved the detection of gas leakage with an aperture of 0.1 mm at a pressure differential of 0.1 MPa; Wang S et al. [17] achieved the detection of gas leakage with a leak rate of 10 L/min; Cruz R P et al. [13] achieved the detection of gas leakage with an aperture of 0.5 mm at a pressure difference of 100 kPa; Liu C et al. [14] achieved gas leak detection with a leak rate of 220 L/min and the detection of gas leakage with a 1 mm pore size at a pressure difference of 0.6 MPa [23]. Compared to them, the proposed sensor in this paper achieves higher leak detection threshold (0.67 mL/s) and smaller detectable leak aperture (0.1 mm) with a small and more compact size. Compared with the software improvement methods, the sensor proposed in this paper is simpler to apply, as it uses realtime circuit to avoid taking up too much computational resources while executing signal processing. The proposed sensor has higher real-time, operability and higher sensitivity.

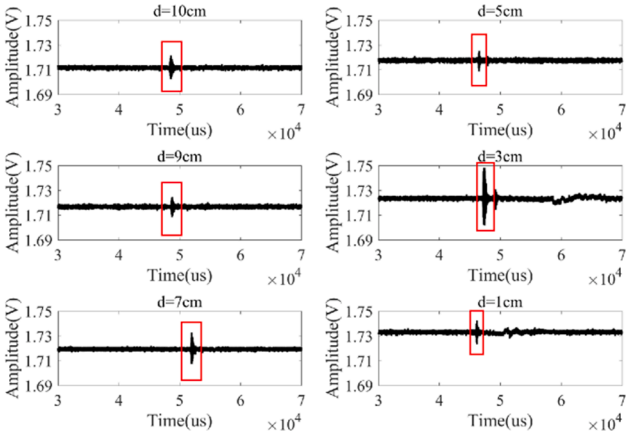

Fig. 12. Acoustic signals generated by bubble bursts.

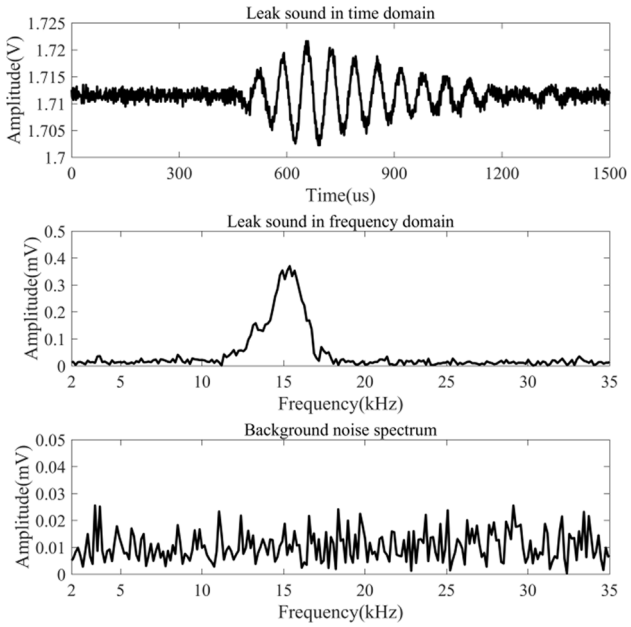

Fig. 13. Bubble burst sound and background noise.

Table 2
A qualitative comparison between other results and this work.

Ref. nos	Nos of mic	Size (mm^2)	Technical features	Sensitivity
[20]	1	–	Vacuum system, leak theory analysis	≥1.6 Pa·m^3/s = 16 mL/s@0.1 MPa
[19]	2 * 2	30 * 30	Transducer parallel circuit	Φ = 0.3 mm
[12]	2 * 2	70 * 70	TDOA, software	0.1 MPa, Φ = 0.1 mm
[17]	1	13 * 13	Lighthill acoustic analogy	≥166 mL/s
[13]	4 * 1	–	Machine learning, software	0.1 MPa, Φ = 0.5 mm
[14]	4 * 1	–	De-noising algorithm	≥3666 mL/s
[23]	1	10 * 10	Machine learning, software	0.6 MPa, Φ = 1 mm
This work	18	20 * 20	Adder circuit	Φ = 0.1 mm, ≥0.67 mL/s

5. Conclusions

A compact microphone array-based sensor capable of detecting very small gas leaks is demonstrated in this study. The results of both numerical calculations and experiments show that the maximum gain of the sensor equals the number of array elements N when the azimuth of the leak source relative to the sensor is close to 0°, whereas the sensor has a gain of $N/\sqrt{2}$ when the azimuth is less than 30° for a 20-kHz frequency. Typical leak detection thresholds for the proposed sensor are 0.83 mL/s for a 0.2 mm leak hole at a distance of 20 cm and 0.67 mL/s for a 0.1 mm leak hole at a distance of 20 cm. The bubble method can be used to enable the sensor to detect a tiny gas leak as small as 0.1 mL/s at a distance of approximately 10 cm based on the sound of the bubble burst sound, even though the bubble is too small to be visible. The proposed sensor can be used for acoustic detection of gas leaks with low leak rates and from very small apertures.

CRediT authorship contribution statement

Jian Li: Funding acquisition, Project administration. **Yulin Li:** Methodology, Writing - original draft. **Xinjing Huang:** Methodology, Funding acquisition, Writing - review & editing, Project administration.

Hao Feng: Conceptualization. **Yu Zhang:** Resources. **Xiaoxia Yang:** Project administration.

Declaration of Competing Interest

The authors declared that they have no conflicts of interest to this work.

Acknowledgments

This work is supported by National Key Research and Development Program of China (No. 2018YFC0808600), National Natural Science Foundation of China (Nos 61803280, 61973227), and Natural Science Foundation of Tianjin (No. 19JCQNJC01700).

References

[1] Li Jiakun, Jin Weiqi, Wang Xia, et al., Review of Gas Leak Infrared Imaging Detection Technology, Infrared Technol. 36 (07) (2014) 513–520.
[2] T. Sakagami, H. Anzai, S. Kubo, et al., Development of a gas leak detection method based on infrared spectrum imaging utilizing microbolometer camera, Proc. Spie 8013 (2011) 357–366.
[3] Sapozhnikova Yelena, Steven J. Lehotay, Review of recent developments and applications in low-pressure (vacuum outlet) gas chromatography, Analy. Chim. Acta 899 (2015) 13–22.
[4] Zhao Wei, Wang Jinlong, Wang Zhaojun, et al., Application of helium mass spectrometry leak detection technology in spent fuel pit transfer cabin, Nondestruct. Test. 42 (04) (2020) 10–14.
[5] Wang Yong, Yan Rongxin, Huang Xining, The principle of the sniffing probe method, Spacecraft Environ. Eng. 27(03) (2010) 351-353+265-266.
[6] Standard Practice for Leaks Using Bubble Emission Techniques, Standard Practice for Leaks Using Bubble Emission Techniques, 2018, Versions: 4.
[7] M.A. Pengfei, S. Tengfei, L. Ronghai, et al., Research on the Method of GIS Gas Leak Detection with Acoustic Emission Technique, High Voltage Apparatus (2018).
[8] Zhang Tao, Study on the Leak Detection of Space Environment Simulator Using Acoustic Emission Technology, Tianjin University, 2014.
[9] Ma Yongcheng, Chen Qingsong, Application of Leak Detection and Location Technology Based on Ultrasonic for Manned Spacecraft, Instrument Tech. Sens. S1 (2009) 341–343.
[10] L.I. Yuxing, L. Cuiwei, Qingdao et al., Advances in leak detection and location based on acoustic wave for gas pipelines, Chinese Sci. Bull. 62(7) (2017) 650-658.
[11] P.S. Murvay, I. Silea, A survey on gas leak detection and localization techniques, J. Loss Prev. Process Ind. 25 (6) (2012) 966–973.
[12] X. Mengjie, W. Tao, Study on gas leakage localization method based on ultrasonic sensor area array, Int. Conf. Adv. Intell. Mechatron. (2017) 136–141.
[13] R.P. Cruz, F.V. Silva, A.M. Fileti, et al., Machine learning and acoustic method applied to leak detection and location in low-pressure gas pipelines, Clean Technol. Environ. Policy (2020) 1–12.
[14] C. Liu, Y. Li, L. Fang, et al., Experimental study on a de-noising system for gas and oil pipelines based on an acoustic leak detection and location method, Int. J. Press. Vessels Pip. 151 (2017) 20–34.
[15] L. Meng, L. Yuxing, W. Wuchang, et al., Experimental study on leak detection and location for gas pipeline based on acoustic method, J. Loss Prev. Process Ind. 25 (1) (2012) 90–102.
[16] H. Jin, L. Zhang, W. Liang, et al., Integrated leakage detection and localization model for gas pipelines based on the acoustic wave method, J. Loss Prev. Process Ind. (2014) 74–88.
[17] S. Wang, X. Yao, Aeroacoustics measurement of the gas leakage rate for single hole, Rev. Sci. Instrum. 91 (4) (2020), 045102.
[18] L. Li, K. Yang, X. Bian, et al., A Gas Leakage Localization Method Based on a Virtual Ultrasonic Sensor Array, Sensors 19 (14) (2019).
[19] Qi Lei, Sun Wei, Sun Lichen, et al., A method of non-contact ultrasonic leak detection, Spacecraft Environ. Eng. 31 (02) (2014) 212–216.
[20] Guo Xin, Yan Rongxin, Ultrasonic leak testing method and its application, Spacecraft Environ. Eng. 27(06) (2010) 739-741+673.
[21] Gong Qichun, Ye Qian, Liu Chengliang, et al., Study and Design of a New Leak-detect System Based on Ultrasonic, Appl. Electron. Tech. 03 (2005) 36–39.
[22] Liu Weiping, Wang Mingquan, Gas Leak Detection by Differential Pressure Method, Mech. Eng. Automat. 01 (2010) 133–135.
[23] R.B. Santos, E.O. De Sousa, F.V. Da Silva, S.L. Da Cruz, A.M.F. Fileti, Detection and on-line prediction of leak magnitude in a gas pipeline using an acoustic method and neural network data processing, Braz. J. Chem. Eng. 31 (1) (2014) 145–153.